
# Investigating lateral porosity effect on air pumping noise from connected road cavities with CFD simulations

Frédéric CONTE[1,a]; Philippe KLEIN[2,a]; Michel BERENGIER[3,b]

[a] IFSTTAR, AME, Université de Lyon/CeLyA, Environmental Acoustics Laboratory, France

[b] IFSTTAR, AME, LUNAM University, Environmental Acoustic Laboratory, France

## ABSTRACT

Several mechanisms induced by the tyre/road interaction contribute to the generation of rolling noise. The road texture has a significant role in this process, together with the possible porosity of the road pavement. The latter may influence the noise sources in the high frequency range in which air pumping is supposed to contribute. Even on dense road surfaces with no vertical porosity, possible air flow allowed by the road texture in the contact patch is equivalent to the effect of a so-called "lateral" porosity which is reckoned to have an influence on the source strength.

In this paper, the effect of this lateral porosity is studied with a modelling approach using Computational Fluid Dynamics (CFD). This approach allows the highlighting of some phenomena occurring in the contact patch such as air compression due to the tyre rolling process or air drainage. Simulations are carried out for a smooth tyre and road textures made of more or less connected cavities. A parametric study is presented in the case of a 2D academic configuration to show the influence of air flow resistance in the contact zone on air pumping noise. Finally, air pumping mechanism is simulated for a 3D configuration.

Keywords: Air pumping, Rolling noise, Porosity I-INCE Classification of Subjects Number(s): 11.7.1

## 1. INTRODUCTION

The interaction between the tyre and the road surface produces several noise generating mechanisms (1). The impacts between the road asperities and the tyre tread cause tyre vibrations which produce the main noise contribution in the low frequency domain. Airflow-related mechanisms, often called air pumping in the literature, are considered to be responsible for the noise in the high frequency domain in usual driving conditions. These mechanisms can be either the volume variation of the cavities of the contact patch due to the tyre rubber deformation or the pressure variations due to air flow induced by the rolling of the tyre (cf. Figure 1).

Road surface characteristics such as texture and porosity may have a strong influence on the rolling noise levels and the relative contributions of the different mechanisms involved. The porosity of the road material (called "vertical" porosity) may induce noise reduction through absorption effect as well as overpressure release in the contact patch. Even on non-absorbing impervious road surfaces, the texture characteristics may substantially modify the voids in the contact patch and create a "lateral" porosity likely to reduce overpressures due to airflow-related mechanisms. As for a porous material, the lateral porosity may be complemented by a permeability characterizing the open lateral porosity or an airflow resistance.

Examples of measurements dealing with the permeability effect on the noise generation can be found in the literature. Ejsmont et al. have highlighted the horizontal porosity effect by showing a noise reduction when the number of longitudinal groove of a tyre tread increases (2). Koike et al. have shown the vertical porosity effect by measuring the pressure reduction in a tyre groove induced by a drainage asphalt pavement (3). The interconnected voids in the contact area allow air flow. So when the air trapped in the contact patch can flow out easily to the outside, the generated noise is lower.

[1] frederic.conte@ifsttar.fr
[2] philippe.klein@ifsttar.fr
[3] michel.berengier@ifsttar.fr

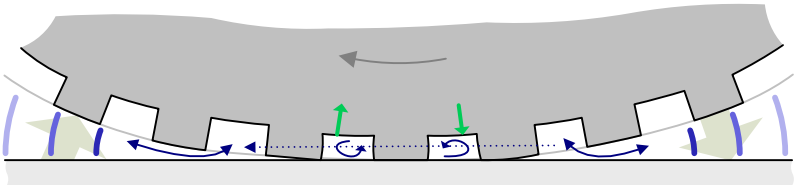

Figure 1 – Sketch of air pumping processes in tyre tread cavities. Green and blue arrows mean respectively tyre tread deformation and aerodynamic processes.

Air flow existing in the contact area decreases the pressure variations which can be generated by the air pumping mechanisms. In this paper, the study focuses on the effect of the permeability of dense road surfaces in the contact patch on air pumping noise. This effect is hereinafter referred to as "lateral porosity". However the behaviour of the noise generation on such surfaces could be extended to all porous road surfaces. CFD simulations of air pumping phenomenon are carried out for 2D and 3D academic configurations.

## 2. APPROACH

### 2.1 Context

Air flow related noise sources involved in tyre/road interaction are difficult to isolate in experiments. Numerical approaches allow the study of complex phenomena such as air flow in a complex geometry. Here Computational Fluid Dynamics (CFD) is used to study unsteady air flow. This work takes place within a general approach introduced in previous studies (4, 5) and presented in (6). This approach consists in modelling aerodynamic mechanisms occurring in the air pumping process likely to induce different possible air flows in the cavities of the contact zone generating pressure variations. Two kinds of mechanisms inducing air flow can be distinguished: the rubber deformation and rigid surface displacements. In this paper only the latter is considered. Surfaces are considered rigid, i.e. without dynamic tyre tread deformation. The only noise generation mechanism is the tyre's rolling creating overpressure in the cavities in front of the contact patch by the boundary layer effect (4-6).

Air flow is considered compressible and viscous. A numerical approach is chosen to handle complex configurations and simulations are carried out with a CFD code based on Navier-Stokes equations.

The strategy consists in taking into account academic configurations in order to understand the phenomena involved. The cavities are included only in the road surface and the tyre tread is considered as smooth. In order to easily investigate the effect of the lateral porosity in the contact zone, a simplified geometry of the road texture is defined as a plane surface with connected cavities. First a 2D parametric study is carried out in order to evaluate the influence of the air flow resistance on the aerodynamic noise generated. Then, the noise radiated by a 3D pervious road texture is simulated.

### 2.2 CFD Model

The CFD model used is similar to the model presented in (5). A smooth rotating tyre rolling over a series of connected cavities included in a smooth road surface is considered. The static deformation shape of a smooth tyre with a radius of 314 mm is taken into account and the reference frame is chosen at the centre of the wheel. Air flows are only generated by the surface displacement and the boundary layer effect. The air flow due to the wheel displacement is not considered.

The Navier-Stokes equations, the mass conservation law and ideal gas law equations are solved. Since the air flow is turbulent, an URANS (Unsteady Reynolds Average Navier-Stokes) approach is used to solve the average flow and model the turbulent component. The RANS model k-ω sst is chosen for its performance to model the flow close to walls (6).

The computational domain is a half-disk in 2D and a quarter of a sphere centred in the middle of the contact area in 3D. A symmetry condition is considered in 3D at the tyre symmetry plane normal to the lateral direction. A non-reflective boundary condition is set at the pressure outlet boundary. It is discretized with respect to fluid dynamics and acoustic wave propagation. The road is modelled as a sliding mesh zone. Equations are discretized with 2$^{nd}$ order accuracy in time and space. Simulations are carried out with the software Ansys Fluent 14.5.

### 2.3 Air flow resistance

The open porosity of the road pavement in the contact patch causes the permeability to air flow. This air flow is curbed but allowed and induces a finite pressure loss. The porosity effect on the flow can be characterized by measuring this pressure loss ΔP for a chosen volumetric flow rate Q.

Air flow resistance $R$ is defined as follows:

$$R = \frac{\Delta P}{Q} \tag{1}$$

The specific air flow resistance $R_s = R/A$ and the air flow resistivity $r = R_s/L$, with $A$ and $L$ respectively the inlet surface and the length in the flow direction of the sample material, are more often considered. The average flow velocity $U$ is defined as $U = Q/A$.

The porosity $\varphi$ considered here for a pervious material is defined by $\varphi = U/v$ where $v$ is the velocity in the pores of the material. It is the porosity related to the permeability, i.e. the porosity seen by the air flow. It differs from the volume porosity which is the percentage of the volume of pores.

The pressure loss can be determined analytically for laminar flow in academic configurations. The Reynolds number $Re$ representing the ratio of the inertial forces to the viscous forces for given flow conditions is used to characterize the flow regime. It is defined by $R_e = \rho VD/\mu$ with $\rho$ the fluid density, $V$ the velocity, $\mu$ the fluid viscosity and $D$ a characteristic length. For low Reynolds number, the pressure loss can be modelled using the Poiseuille's law.

In this paper, air flow resistivity is calculated analytically and numerically in order to check hypothesis done in analytical models and to evaluate in which velocity range inertial forces cannot be neglected. Numerical simulations of air flow resistance are carried out for static flow conditions.

## 3. STUDY OF THE POROSITY EFFECT ON AIR PUMPING NOISE IN 2D

As a first step, the lateral porosity effect is studied for 2D configurations in order to save computational time and to be able to carry out a parametric study. The defined surface consists of a series of interconnected open cavities. The connection between cavities is made with a thin air film. Air flow resistance is varied with the thickness of the air film. CFD simulations of air pumping mechanism are carried out. Finally the corresponding air flow resistivity is evaluated for each thickness value.

### 3.1 Configuration

The shape and size of the cavities are chosen to be similar to cavities of smooth actual roads. The cavities considered have the same triangular shape 2 mm deep and 2 mm wide. They are randomly distributed (cf. Figure 2). The distance between adjacent cavities varies from 2 to 8 mm with an average distance of 5 mm. The parameter chosen to control air flow resistance in the contact patch is the thickness $h$ of the air film connecting the cavities. In 2D, this air film should be at the top of the cavities. However this means that there would not be any contact between the tyre and the road and thus would not be-realistic. Therefore the air film is placed slightly under the contact height at 0.3 mm.


Figure 2 – Sketch of the geometry of the series of connected cavities

The parametric study is performed for a rolling speed of 80 km/h. The thickness of the air film varies from 0 mm (no connections) to 0.5 mm. Six thickness values are considered and listed in Table 1. The corresponding porosity is determined relative to the depth of the cavities so $\varphi = h/2$ mm.

Table 1 – Channel thickness and corresponding lateral porosity for the studied configurations

| $h$ (mm) | 0 | 0.02 | 0.05 | 0.1 | 0.2 | 0.5 |
|---|---|---|---|---|---|---|
| $\varphi$ (%) | 0 | 1 | 2.5 | 5 | 10 | 25 |

### 3.2 Air pumping simulation

Simulations are carried out for the six configurations. The analysis focuses on the calculated pressure inside cavities, air velocity in the connections and sound pressure at several locations.

Figure 3 (a) presents the pressure evolution calculated in a single road cavity during the tyre passing for each configuration. Three phases of the mechanism can be distinguished: the compression phase, the contact phase and the release phase. The strongest overpressure is obtained for closed cavities and is maintained during the contact. For the smallest channels the over pressure is smaller but it is also maintained. For these cases a resonance is induced in the cavity at the release of the overpressure. For larger channels, air flow resistance is weak enough to allow air flow on the full contact length. Then the overpressure generated at the leading edge decreases progressively during the contact. Figure 3 (b) shows the pressure waves propagating at the front and the rear of the contact zone for the case of the channel 0.2 mm thick.

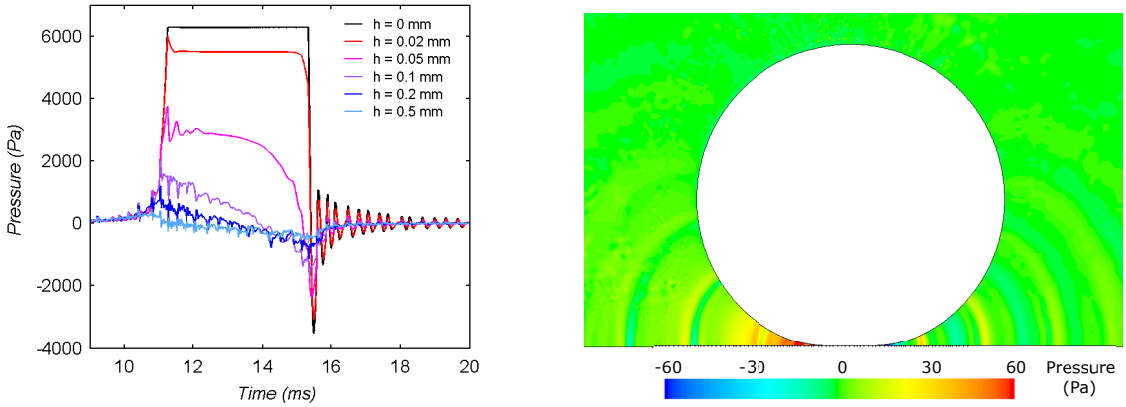


(a) Pressure evolution calculated at the bottom of a cavity for several channel thicknesses

(b) Pressure field around the tyre at a given time for the case $h = 0.2$ mm

Figure 3 – Results of the pressure calculation for the 2D configuration of a series of connected cavities

Figure 4 shows the sound pressure levels calculated at 20 cm at the rear and at the front. At the rear of the contact patch, the pressure magnitude is stronger for small channels because of the Helmholtz resonance at the opening of the cavities. The maximum of the noise spectra is situated between 3 and 5 kHz. There is a decrease of more than 25 dB of the maximum level between the closed cavities series and the case of the 0.5 mm thick channel. This difference is about 10 dB at the front. For the larger channels, the noise spectra shapes calculated at the rear and at the front are similar. The noise at the front is due to overpressures generated at the leading edge and expelled at the closure of the cavities (4, 6). Figure 4 (b) shows that the noise spectrum is affected by the road lateral porosity for the largest channels only.

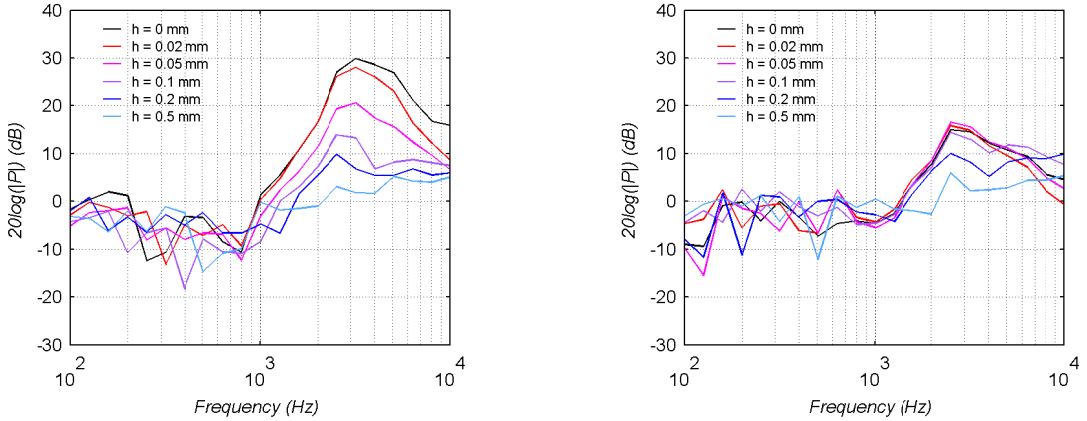


(a) Third octave band pressure spectra at the rear

(b) Third octave band pressure spectra at the front

Figure 4 – Sound pressure spectra ($P_{ref} = 1$ Pa, add 94 dB for $P_{ref} = 20$ µPa) calculated at 20 cm at the rear and at the front of the contact zone for several configurations

The normal relative velocity averaged on a vertical section is calculated in the air film connecting the cavities. The evolution of the velocity during the passing of the tyre is shown in Figure 5. Figure 5 (a) presents the average velocity $v$ in the channel and Figure 5 (b) the average velocity $U$ in the contact patch for a constant section of 2 mm high corresponding to the cavity depth (cf. section 2.3). $U$ is proportional to the flow rate through the contact patch. In the channels, the relative velocity is negative

at the front and at the rear of the contact patch where air is respectively pushed and aspirated by the tyre. In the contact patch, this velocity is positive because air is going from the overpressure at the front toward low pressure at the rear. This velocity has a constant average for large channels. The velocity increases at the end of the contact patch for thin channels causing the pressure loss shown in Figure 3 (a). The flow rate is more important for large channels with lower air flow resistance. The corresponding Reynolds number for the largest channel is about 300; thus the flow is laminar in the contact patch for these configurations. It is to be noticed that air flow velocities are more important than acoustic velocities often used to characterize such porous materials.

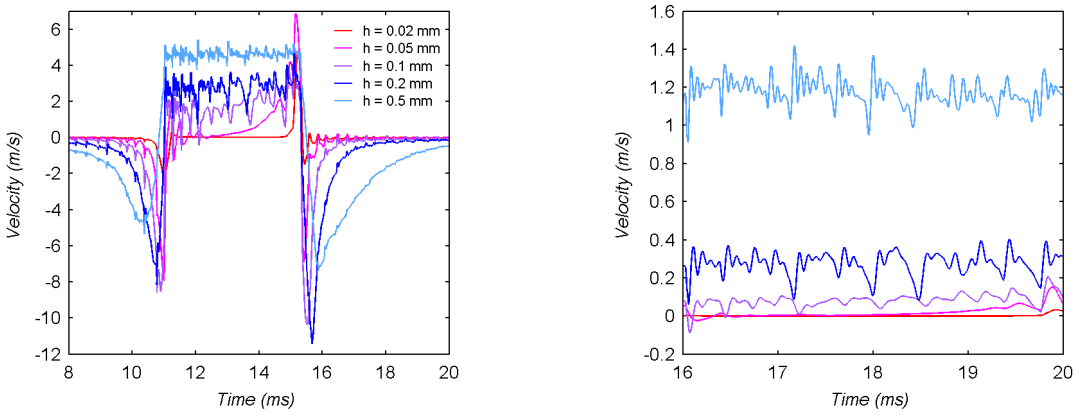


(a) Flow velocities $v$ in the channel (b) Average flow velocity $U$ in the contact zone

Figure 5 – Evolution of the relative air flow velocity in the contact zone for connected cavities configurations

Finally the total sound pressure level at the rear and at the front is plotted as a function of the channel thickness in Figure 7 (a). As seen in Figure 4, the noise decrease is more important at the rear. Indeed, small thickness affects only the noise due the resonances at the rear. Above 0.1 mm the noises from the rear and from the front behave similarly. The noise generated at the front is about 2 dB stronger with a similar spectrum shape (cf. Figure 4). This noise propagating through the channel is radiated at the rear (5).

The noise due to the resonance of the cavities at the rear of the contact patch which is dominant for almost closed cavities is rapidly reduced for a pervious road profile. Thus for 2D configurations, the noise is mainly generated at the leading edge radiating at the rear through the contact patch. This noise is also reduced when the channel thickness increases.

### 3.3 Air flow resistivity evaluation

For air flow with low Reynolds number in a channel, the velocity profile normal to the flow direction has a parabolic shape. The pressure loss due to friction forces can be modelled with the Poiseuille's law. For a flow between two parallel plates, the pressure loss $\Delta P$ can be written as follows:

$$\Delta P = \frac{12\mu LV}{h^2} \tag{2}$$

where $L$ is the length of the plates, $h$ the distance between them and $V$ the mean flow velocity. Therefore, for low flow velocities air flow resistivity (defined in section 2.3) due to a channel does not depend on the velocity. For the case of the road profile described in section 3.1, air flow resistivity in the contact patch can be modelled as follows:

$$r = \frac{12\mu}{\varphi h^2}\frac{L_p}{L} + b \tag{3}$$

with $L_p$ the total length of the connecting channels, $L$ the length of the road profile. $\varphi$ is the porosity defined by $\varphi = U/v$ where $v$ is the velocity in the channel. The last term $b$ stands for the contribution of the triangular cavities to the total resistivity of the road profile.

In order to more precisely evaluate the air flow resistivity for the road profile considered in realistic conditions, additional CFD simulations are carried out. Calculations are done for material samples 10 cm long for each channel thickness and several velocities. Air flow is considered static, laminar and incompressible. This last hypothesis is not taken into account for thin channels for which the

compressibility of air is not negligible (cf. Figure 6).

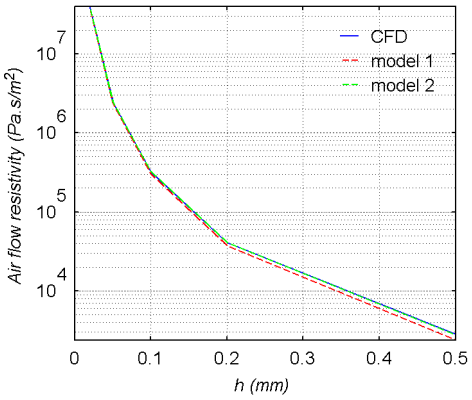


(a) Air flow resistivity calculated for incompressible flow at velocity $U = 0.01$ m/s – comparison of CFD results and analytical models

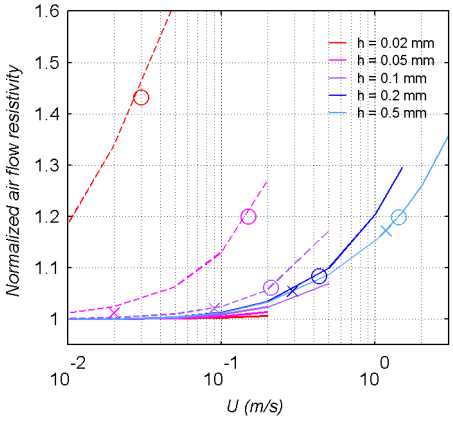


(b) Normalized air flow resistivity calculated for incompressible flow (-) and compressible flow (--). (x) and (o) stand for respectively the values in average and maximum flow conditions during the tyre rolling calculated in section 3.2

Figure 6 – Air flow resistivity calculated with CFD simulations for several flow velocities

Figure 6 (a) shows the air flow resistivity calculated for each configuration and an incompressible flow at the velocity of 0.01 m/s. Results from CFD simulations are compared to the results of the analytical model (equation (3)). Air flow resistivity is very strong for the thinnest channel and decreases rapidly when the thickness of the channel increases. The model 1 corresponds to the resistivity only due to the channels ($b = 0$). The difference with respect to the CFD model ranges from 4% to 15% for respectively the smallest and the largest thickness. This difference can be approximated by the function $\Delta r = 1.06\varphi^{-2.51}$. This should mainly correspond to the contribution of the cavities $b$. This additional term is introduced in model 2.

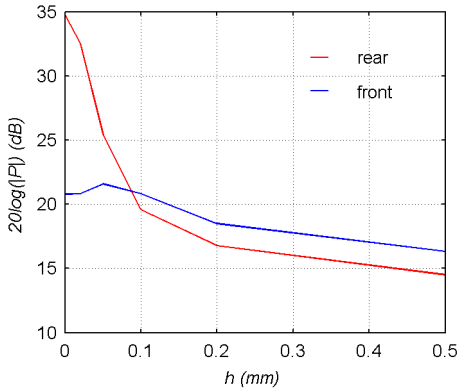


(a)

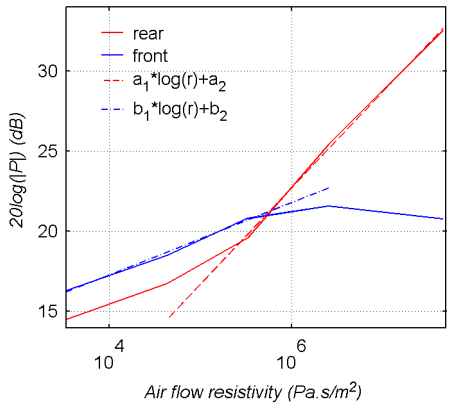


(b)

Figure 7 – Sound pressure level ($P_{ref} = 1$ Pa, add 94 dB for $P_{ref} = 20$ µPa) calculated at 20 cm at the rear and at the front of the contact zone as a function of the channel thickness (a) and air flow resistivity due to the lateral porosity (b)

The air flow resistivity normalized by the value calculated at the 0.01 m/s velocity for an incompressible flow is drawn in Figure 6 (b) as a function of the flow velocity. For incompressible flow and low velocities, air flow resistivity is almost constant for all configurations as described by the Poiseuille's law. At 0.1 m/s, the variation is less than 2 %. Above 0.1 m/s air flow resistance increases more with the velocity. Figure 6 (b) shows an important compressible effect for small channel thicknesses ($h < 0.1$ mm) and high velocities. Air flow resistivity values corresponding to average and maximum velocity flow conditions during tyre's rolling simulations (cf. Figure 5 (b)) are also plotted. In rolling condition, the compressible effect can be neglected (for the thinnest channel flow is allowed

only at the edge of the contact patch). However the velocity effect should be taken into account for the largest channels.

The sound pressure levels at the front and rear of the contact zone are plotted against the thickness values (Figure 7 (a)) and corresponding air flow resistivity values (Figure 7 (b)). For low air flow resistivity, the noise which is generated at the front propagates towards the rear through the contact patch and the pressure levels at the front are higher of about 2 dB than those at the rear. They can be modelled by the function $b_1 \log r + b_2$ with $b_1$ = 2.25 and $b_2$ = 8.31. For higher resistivity values, noise at the front stabilizes at the same level while the noise due to cavity resonances at the rear increases significantly. In this range it can be modelled by the function $a_1 \log r + a_2$ with $a_1$ = 6 and $a_2$ = -13.3.

## 4. CASE OF A 3D DENSE ROAD SURFACE

3D simulations of air pumping have been already carried out for closed cavities or a single open groove (5). The effect of the lateral porosity of the road on the air pumping noise is considered here in the simulation of the air pumping process for a 3D road texture. These aim at evaluating the noise generated by the aerodynamic mechanism considered for a pervious road surface and calculating the air flow resistivity of this surface.

### 4.1 Configuration

The road texture chosen is based on a road surface introduced in previous projects (7, 8) which is a low noise dense road surface with a controlled road texture (9). It consists of crossing oblique grooves with a Gaussian shape and a random distribution. This surface is supposed to reduce strongly the noise due to tyre vibrations as well as air pumping. This is a dense road surface but the grooves provide a lateral porosity to the surface and allow the drainage of the contact patch.

For reducing computational cost the rolling process is performed over a short road sample and a regular distribution of the groves is chosen. The road texture is also simplified considering a rectangular shape of the grooves with the same section area. These grooves have a square section with a width $h$ = 1 mm. The distance between each other is $d$ = 7 mm and they have an angle of 45° with the travel direction. The road sample considered has a half width of 10 cm and a length of 30 cm. A sketch of the groove pattern is given in Figure 8 (a) and the geometry of the road sample and the tyre near the contact zone is shown inFigure 8 (b).

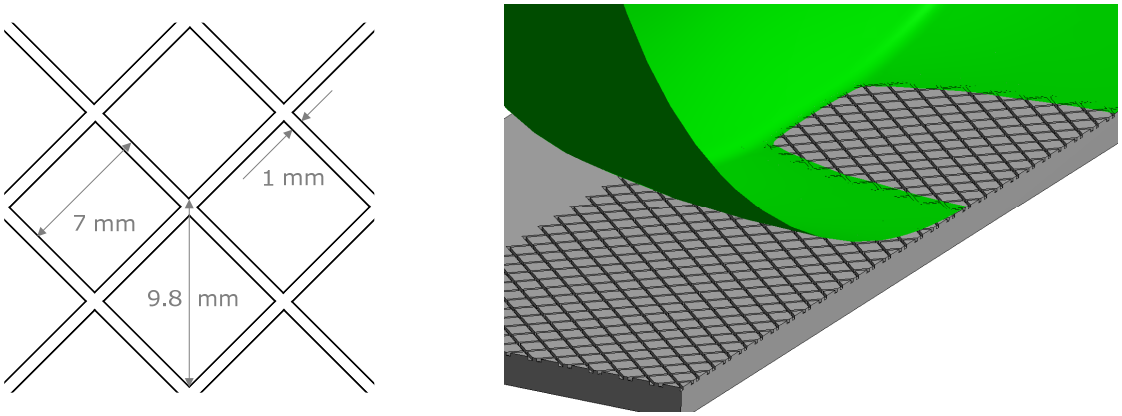


(a) Sketch of the groove pattern

(b) Geometry of the tyre and road considered in the CFD model near the contact zone

Figure 8 – Geometry of the 3D road texture

### 4.2 Air pumping simulation

A simulation is carried out for a tyre passing at 80 km/h. Figure 9 (a) presents the pressure evolution calculated at the bottom of the grooves during the contact. The pressure signals calculated at different lateral locations in the contact zone have a similar shape. An overpressure is generated at the leading edge and the pressure drops at the entrance in the contact area. This overpressure is shown in Figure 9 (b) in front of the leading edge. It is to be noticed that the overpressure about 200 Pa in front of the contact caused by the air flow around the tyre due to wheel displacement (6) negligible for closed

cavities and not taken into account here may have an influence on the noise level in this case.

Then the pressure oscillates and decreases progressively during the contact to create a depression which suddenly disappears at the exit of the contact without resonance of the grooves at the rear. The receivers situated at 7 cm and 9 cm pass respectively at the edge of the contact patch and outside. This behaviour is similar to the case of the 2D road surface having the largest channel (cf. Figure 3 (a)).

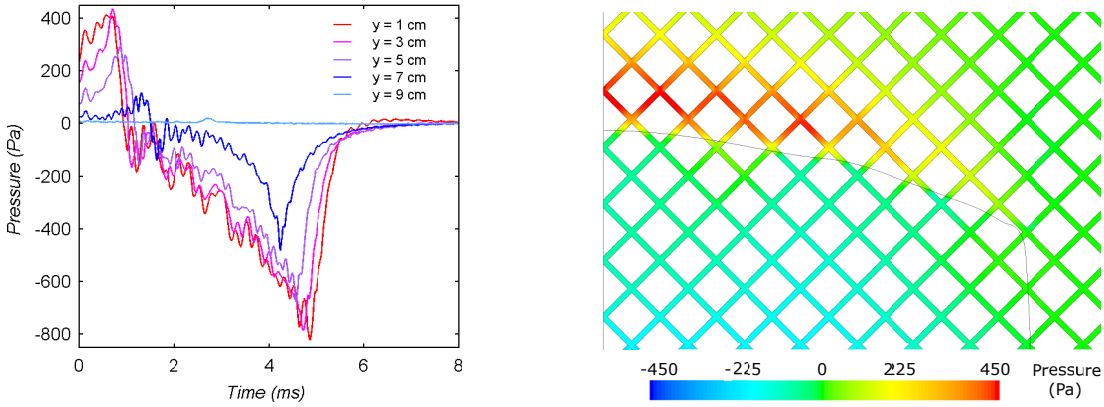


(a) Pressure evolution at several lateral distances from the centre of the contact zone

(b) Pressure field at a given time at the front of the contact patch

Figure 9 – Pressure calculated at the bottom of the grooves in the contact zone

The pressure evolution and the corresponding noise spectrum are also calculated at several receiver locations around the tyre. The results are presented in Figure 10 for receivers at a distance of 20 cm from the contact centre. The 4 receivers are located at the front of the contact zone, on the side at 60° and 120° relative to the travel direction and at the rear. The noise is weaker on the side of the tyre and the maximum is reached at the front. The sound pressure spectra are made of several peaks. The first frequency corresponds to the parallel grooves passing frequency under the tyre of 2245 Hz. The frequencies of the other peaks are multiples of this frequency. The second peak is the most important and reaches 85 dB at the front. Its frequency correspond the passing frequency of the groove crossing in the contact zone of 4490 Hz. Indeed these junctions are offset relative to each other by a half-distance (cf. Figure 8 (a)). Aerodynamic pressure fluctuations may contribute to the pressure spectra calculated at 20 cm in the low frequency range.

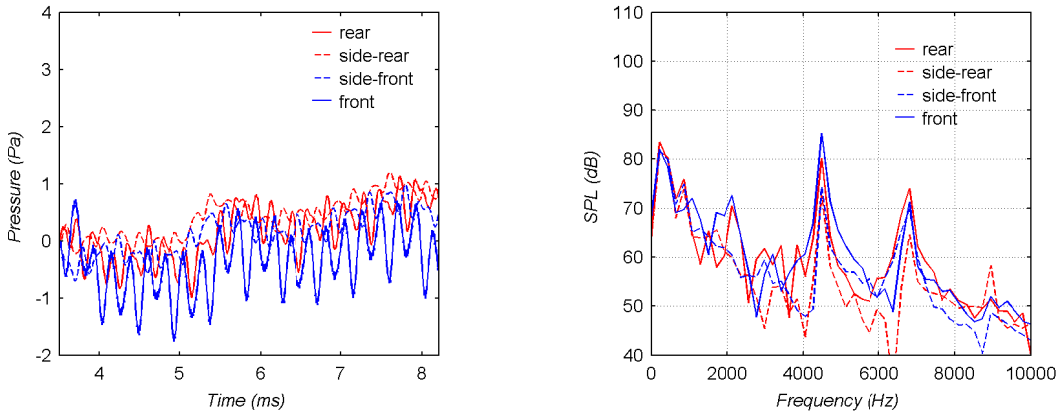


(a) Pressure evolution

(b) Sound pressure spectra

Figure 10 – Pressure evolution and sound pressure spectra ($P_{ref}$ = 20 µPa) calculated at 4 locations around the contact patch at 20 cm from the centre

For this road surface made of small connecting grooves noise is generated mainly at the front of the contact patch due to the overpressure created at the leading edge and expelled at the closure of the grooves by the tyre tread (4-6). This noise can be radiated through the contact zone (5). Sound pressure level due to this mechanism remains quite low at this distance.

Figure 11 (a) shows the evolution of the relative flow velocity in the grooves. For the groove sections passing in the contact patch, the behaviour of the air flow is similar to the flow in the 2D configuration. The air velocity is only positive and almost constant in the contact patch. There is an

asymmetry in the flow depending on the orientation of the grooves on the edges of the contact patch. On the side, expulsion and suction of air occur in opposition on the crossing grooves. The Reynolds number in the contact zone does not exceed 800 so air flow regime is laminar. Figure 11 (b) shows the evolution during the contact of the average velocity corresponding to the flow rate in the contact patch. This velocity increases from about 0.3 m/s to 0.58 m/s between the entrance and the exit of the contact area.

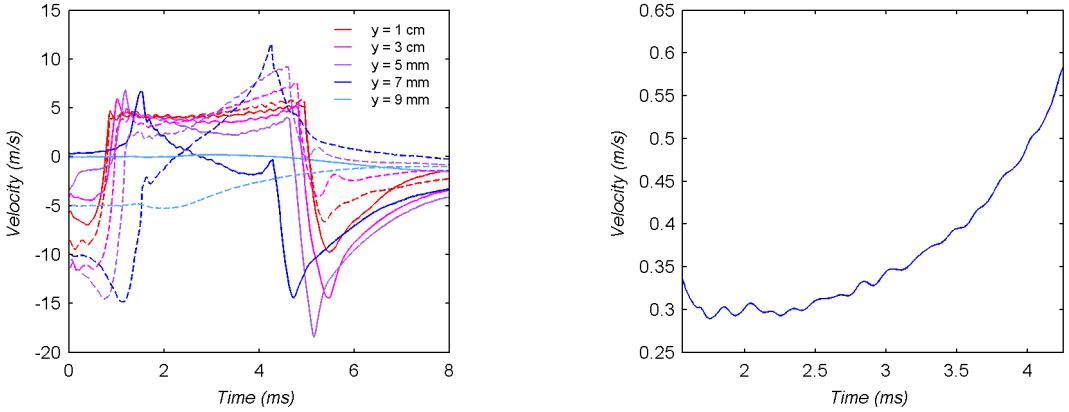


(a) Average flow velocities $v$ in the grooves at 45° (-) and 135° (--) relative to the travel direction

(b) Average flow velocity $U$ in the contact zone

Figure 11 – Evolution of the relative air flow velocity in the contact zone for connected cavities configurations

### 4.3 Air flow resistivity evaluation

As for the configuration of a 2D channel, the pressure loss due to air flow resistance in a pipe can be modelled for low Reynolds number with the Poiseuille's law. The pressure loss $\Delta P$ can be written in this case as follows:

$$\Delta P = \frac{32\mu LV}{D_h^2} \tag{4}$$

where $L$ is the length of the pipe, $D_h$ the hydraulic diameter and $V$ the mean flow velocity. The 3D road texture considered in the contact patch can be modelled by a material made of several pipes. Then air flow resistivity can be written as follows:

$$r = \frac{32\mu}{\varphi h^2}\frac{L_p}{L} + b \tag{5}$$

with $L_p = \sqrt{2}L$ the length of the grooves, $L$ the length of the sample. $\varphi$ is the porosity defined by $\varphi = U/v$ where $v$ is the velocity in the groove. In this case $\varphi = 2h/d = 28.6\%$. $b$ is the contribution of the grooves crossing to the total resistivity of the road profile. If this contribution is neglected air flow resistivity $r$ = 2831.4 Pa.s/m$^2$.

Air flow resistivity is also calculated with a CFD model for several flow velocities. Simulations are performed for a material sample 10 cm long and 10 cm wide. Air flow is considered static, laminar and incompressible. Results are presented in Figure 12. The evolution of air flow resistivity is almost linear and can be modelled by the function $c_1 U + c_2$ with $c_1$ = 7.73·10$^3$ and $c_2$ = 3.21·10$^3$. At low velocity the velocity dependency is slightly weaker. At 0.01 m/s, the analytical model without crossing grooves contribution (b = 0) underestimates air flow resistivity of 17%.

The flow conditions in the contact patch for tyre rolling are presented in Figure 11 (b). It is to be noticed that air flow is not uniform in the contact patch due to side effects. At minimum and maximum rolling conditions, resistivity corresponds respectively to 1.6 and 2.3 times the resistivity calculated at 0.01 m/s. The velocity effect is therefore not negligible in the estimation of the air flow resistivity involved in air pumping mechanism.

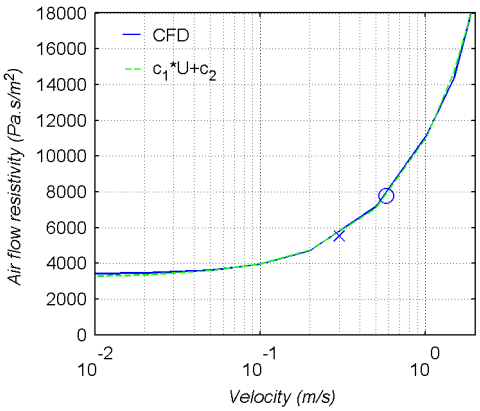


Figure 12 – Air flow resistivity calculated with CFD simulations for several flow velocities for an incompressible flow. (x) and (o) represent respectively minimum and maximum flow conditions for tyre rolling calculated in section 4.2

## 5. CONCLUSIONS

Even on dense road surfaces, the lateral porosity due to the road texture in the contact patch influences aerodynamic noise sources. A CFD model is implemented in order to investigate the effect of the lateral porosity on the air pumping noise. The 2D parametric study of the noise generated by the tyre rolling over a series of connected cavities highlights the effects of the air flow resistivity in the contact patch on the noise radiated from the leading and trailing edges. A simulation is carried out for a 3D dense road surface. Noise is mainly generated at the leading edge and radiated despite the permeability induced by the lateral porosity. The noise level remains rather low in this particular case.

The study of the air flow resistivity in the contact patch for several configurations brings to the light the influence of air flow velocity in the range encountered during the rolling in the contact patch.

## ACKNOWLEDGEMENTS

Authors gratefully acknowledge the financial support from the French Environment and Energy Management Agency (ADEME) within the framework of the DEUFRAKO project ODSurf.

This work was performed within the framework of the Labex CeLyA of Université de Lyon, operated by the French National Research Agency (ANR-10-LABX-0060/ ANR-11-IDEX-0007).

## REFERENCES

1. Sandberg U and Ejsmont J.A. Tyre/road noise reference book. Kisa, Sweden: Informex; 2002. 616 p.
2. Ejsmont J.A., Sandberg U, Taryma S. Influence of the tread pattern on tire/road noise. SAE technical paper series; Soc. of Autom. Eng. SAE papers N°841238, 1984.
3. Koike H, Fujikawa T, Oshino Y, et al. Generation mechanism of tire/road noise – Part 2: pipe resonance in tread groove of tire. Proc. INTER-NOISE 1999; 6 - 8 December 1999; Fort Lauderdale, USA 1999. p.199-203.
4. Conte F and Jean P. CFD modelling of air compression and release in road cavities during tyre road interaction. Proc. Euronoise 2006; 30 may - 1 June 2006; Tampere, Finland, 2006. 6 p.
5. Conte F and Klein P. 3D CFD modelling of air pumping noise from road cavities with constant volume. Proc INTER-NOISE 2013; 15-18 September 2013; Innsbruck, Austria, 2013. 10 p.
6. Conte F, Modélisation CFD du phénomène acoustique de pompage d'air dans un contact pneumatique/chaussée. Doctoral thesis (in French). France: INSA Lyon; 2008. 270 p.
7. EC project: Integrated Tyre and Road Interaction (ITARI). FP6-SUSTDEV 506437. Final report, 2007.
8. DEUFRAKO project: Prediction and Propagation of Rolling Noise (P2RN). Final report, 2009.
9. Beckenbauer, T. Road surface and method for the production thereof. Patent WO 2009/130222 A1, Oct. 21, 2009.